Uniform partitions and a dimensions spectrum for lacunar measures

2002 J. Phys. A: Math. Gen. 35 1871

(http://iopscience.iop.org/0305-4470/35/8/305)

INSTITUTE OF PHYSICS PUBLISHING JOURNAL OF PHYSICS A: MATHEMATICAL AND GENERAL

J. Phys. A: Math. Gen. **35** (2002) 1871–1884 PII: S0305-4470(02)22221-0

Uniform partitions and a dimensions spectrum for lacunar measures

R Santoro[1], N M Maraldi[1], S Campagna[2] and G Turchetti[3,4]

[1]Istituto di Citomorfologia Normale e Patologica CNR c/o IOR, Via di Barbiano 1/10 Bologna, Italy
[2]CINECA, Via Magnanelli 6/3 Casalecchio di Reno, Bologna, Italy
[3]Dipartimento di Fisica della Università, Via Irnerio 46 Bologna, Italy
[4]Centro Interdipartimentale L Galvani, Università di Bologna, Italy

Received 23 February 2001, in final form 18 December 2001
Published 15 February 2002
Online at stacks.iop.org/JPhysA/35/1871

Abstract

A multifractal analysis has been proposed to investigate complex systems, which exhibit a nonuniform local structure. Multifractal measures are normalized mass distributions inhomogeneous at every scale. To every point P is associated the exponent α of the power law r^α describing the asymptotic behaviour as $r \to 0$ of the mass of a sphere of radius r and centre P. The measure properties are specified by the dimension spectrum $f(\alpha)$ of the set of points P with the same scaling exponent α. This spectrum is nontrivial even when the mass distribution has no holes (measure with Euclidean support) and the box counting dimension is an integer. In this case it can be evaluated by considering a sequence of uniform grids, whose spacing decreases as 2^{-n}, known as uniform partitions. We consider here a family of iterated function system fractal measures with support on the unit square with random defects specified by three parameters: a scale ϵ, a probability p and an attenuation factor η. Given a partition with a diameter less than ϵ any cell is chosen with probability p and its mass is multiplied by η: the corresponding pre-measure is obtained after normalization. In all the examples examined the $f(\alpha)$ spectrum appears to widen monotonically as η decreases. This result suggests the possibility of using the method to detect the presence of defects in sponge-like structures, such as cancellous bone (sponge-like), by analysing their radiographs since the grey intensity is related to the mass density of the structure. A widening of the $f(\alpha)$ spectrum is indeed observed in osteoporotic bone radiographs compared to normal bone radiographs. This may be attributed to the rarefaction of the cancellous bone.

PACS numbers: 05.45.Df, 87.59.-e, 87.58.Xs

(Some figures in this article are in colour only in the electronic version)

1. Introduction

The local properties of fractal measures are specified by the scaling exponents of spheres and the uniform partitions provide an algorithm to evaluate the spectrum of exponents [1–5]. Convergence of the algorithm to the generalized dimensions $D(q)$ has been proved for positive values of q, the result being the same as for dynamic partitions [6, 7]. An optimal complexity algorithm was developed to compute the uniform partitions in [8]. The numerical convergence of the algorithm for positive values of q was confirmed and evidence was given for convergence, when q is negative, only for measures whose support is the unit square or whose uniform partitions are a subset of the dynamic partitions. For any other measure with fractal support the convergence is very poor for $q < 0$; the possible limit values $D_*(q)$ differ from the dimensions $D(q)$ obtained with dynamic partitions [8]. A modified algorithm, based on extended boxes, has been proposed to overcome the difficulties with $q < 0$ for the measures with fractal support [9]. Another approach, based on wavelet transforms, has also been considered [10]. Since we deal with digitized images, we assume the underlying measure has a Euclidean support (the unit square) and we used the algorithm [8] having an optimal computational complexity. The partition function $Z^{(n)}(q)$ for a lattice of side 2^{-n} is determined recursively and for a measure defined by an array of $2^N \times 2^N$ pixels the computational complexity is proportional to 2^{2N+2}. The values of $\log_2 Z^{(n)}(q)$ are close to a straight line (discarding the lowest n). The slope is determined by the least square fit method. The fractal measures we have considered to test the method are the iterated functions systems (IFS), for which the dimension spectrum is known analytically [11]. Rather than the dimensions spectrum $D(q)$ we examine the spectrum $f(\alpha)$, defined by the Legendre transform of the concave function $\tau(q) = (q-1)D(q)$. The function $f(\alpha)$ is the Hausdorff dimension of the set of points, for which the scaling exponent of the measure is α, and describes the spread of scaling exponents through the support of the measure.

Having in mind some biomedical applications we have analysed the variation of the spectrum caused by the introduction of random defects in the fractal measures [12]. These defects are characterized by a scale ϵ (the diameter of the defect), by a probability p of the defect to appear and by an attenuation factor η ranging from 0 (lacunes) to 1 (no defect). The defects are meant to simulate the effect of osteoporosis in a cancellous (sponge-like) bone [13], whose radiographic image is assumed to correspond to a fractal measure. The scale and the probability are varied to simulate different stages of the pathological degeneration. The key issue is to detect, in this mathematical model, the sensitivity of the spectrum of local exponents to the size and the probability of defects, namely to the degree of the pathological state.

Osteoporosis is a pathology which causes a rarefaction of the trabecular structure of the bone. The definition of a model correctly describing this effect is a very hard task. First of all one should describe the 3D structure of the cancellous bone, which is like a porous material, and of the organic material filling the pores, specifying what kind of changes occur in the osteoporotic state. A model based on 3D fractal measures should be compared with 3D tomographic images of the bone. The 3D reconstructions are not considered in routine clinical tests. In contrast, the 2D fractal measures can be compared with ordinary x-radiographs. The 3D program is beyond the scope of the analysis we present here.

Keeping in mind that the 3D approach to the problem should be considered in the future, we have analysed the ordinary x-radiographs. They provide a projection on a plane of the solid structure of the cancellous bone and of the soft material filling it. The 2D fractal measure with defects we propose should describe the basic structure of these radiographs concerning the changes induced by osteoporosis. As a mathematical model we consider an IFS measure where the defects are introduced by reducing, according to the attenuation factor η, the pre-

measure of the elements of the dynamic partitions of diameter less than ϵ, chosen according to a probability p. A normalization procedure is applied at any step of the generating process to obtain the sequence of pre-measures, whose limit is the IFS measure with defects. The defects we consider are not lacunae (unless $\eta = 0$) but only a random attenuation of the measure, occurring below a given scale and with an assigned probability. As a consequence we believe that the problems encountered by the uniform partition algorithms in the case of measures with fractal support are avoided.

This is certainly true for low attenuation namely for η close to 1 or for both η and p small. For $\eta = 0$ the measure becomes lacunar and has a fractal support. When η approaches zero the proposed algorithm should still converge to the right measure, however, in the absence of estimates on the convergence speed, we cannot exclude that, for negative values of q, it slows down very rapidly with η when $\eta \to 0$. In this case the numerical results obtained at a finite order are no longer reliable, unless the probability p of the defect with low η is very small, as in the chosen examples. In future work we plan to investigate the $\eta \to 0$ limit using the algorithms proposed in [9, 10], which are claimed to be convergent for $q < 0$ also in the case of measures with a fractal support.

Since the direct quantitative comparison of the spectra is not practical we have examined the first moments. To this end the whole spectrum must be known and in our case an extrapolation to reach the end points $\alpha_\pm$, where $f(\alpha)$ vanishes and has a vertical tangent $f'(\alpha) = q = \pm\infty$, is needed. The occurrence of negative dimensions allowing $f(\alpha)$ to vanish before the end-points $\alpha_\pm$ appears to be extremely unlikely even for η very close to zero. The interpolation is made with cubic splines plus two arcs of the algebraic curve to allow for vertical tangents at the ends of the interval where the spectrum is defined.

We have applied the proposed method to analyse a sample of normal and osteoporotic bone radiographs. The widening of $f(\alpha)$ spectrum observed in the case of the osteoporotic bone radiographs is similar to the change occurring in the IFS measures when the defects are introduced and can be attributed to the rarefaction of the bone trabecular structure.

2. Uniform partitions

We consider a system $M = (M_1, \ldots, M_s)$ of linear maps with statistical weights $(p_1, \ldots, p_s)$. Letting

$$M_i(\boldsymbol{x}) = \lambda_i R(\alpha_i)\boldsymbol{x} + \boldsymbol{b}_i \qquad 0 < \lambda_i < 1 \qquad \boldsymbol{x} \in I = [0,1]^d \tag{2.1}$$

where R denotes an orthogonal matrix, we assume that the images $I_j = M_j(I)$ of the unit cube are disjoint. The iterations $M^n(A_0)$ converge for any $A_0 \subseteq I$ to a fractal attractor $\mathcal{A}$. We define the partitions $\mathcal{I}^{(n)}$ of the cube by the recurrence $\mathcal{I}^{(n)} = M(\mathcal{I}^{(n-1)})$ where $\mathcal{I}^{(0)} = I$ and the partitions of $\mathcal{A}$ by $\mathcal{A}^{(n)} = \mathcal{I}^{(n)} \cap \mathcal{A}$. Any partition is the union of s^n disjoint sets

$$\begin{aligned} \mathcal{I}^{(n)} &= \bigcup_{k_n,\ldots,k_1} I_{k_n,\ldots,k_1} \qquad I_{k_n,\ldots,k_1} = M_{k_n} \cdots M_{k_1}(I) \\ \mathcal{A}^{(n)} &= \bigcup_{k_n,\ldots,k_1} A_{k_n,\ldots,k_1} \qquad A_{k_n,\ldots,k_1} = I_{k_n,\ldots,k_1} \cap \mathcal{A}. \end{aligned} \tag{2.2}$$

A sequence $\mu^{(n)}$ can be defined by assigning the value it takes on the sets $I_{k_n,\ldots,k_1}$

$$\mu^{(n)}(I_{k_n,\ldots,k_1}) = p_{k_1} \cdots p_{k_n} \tag{2.3}$$

where $p_1 + \cdots + p_s = 1$. We define a pre-measure μ on $\mathcal{A}$ by assigning the value it takes on the sets $A_{k_n,\ldots,k_1}$ according to $\mu(A_{k_n,\ldots,k_1}) = \mu^{(n)}(I_{k_n,\ldots,k_1})$. The invariance of the measure with respect to M follows from the definition (2.3) and reads $\mu(M(A)) = \mu(A)$. The dimensions

spectra are introduced in the framework of the thermodynamic formalism as well. The free energy for the dynamic partitions of an IFS is defined by

$$\mathcal{F}_{D}(q,\tau)=\lim_{n\to\infty}\frac{1}{n}\log\sum_{k_n,\ldots,k_1}\frac{(p_{k_1}\cdots p_{k_n})^q}{(\lambda_{k_1}\cdots\lambda_{k_n})^\tau}=\log\sum_{j=1}^{s}p_j^q\lambda_j^{-\tau} \tag{2.4}$$

where $\lambda_{k_1}\ldots\lambda_{k_n}=\delta(A_{k_n\ldots k_1})$ is the diameter of the set $A_{k_1\ldots k_n}$. The dynamic free energy $\mathcal{F}_{D}$ vanishes at the scaling exponents $\tau(q)$ of the correlation integrals. The spectrum of generalized dimensions is defined by $D_q=\tau(q)/(q-1)$. Moreover $D_0=-\tau(0)$ is the Hausdorff dimension. Indeed the Hausdorff measure is defined on coverings $\mathcal{B}_\epsilon$ with sets B_i of diameter $\epsilon_i\leqslant\epsilon$ according to

$$H(\epsilon,\beta)=\inf_{\mathcal{B}_\epsilon}\sum_i\epsilon_i^\beta \tag{2.5}$$

and the limit for $\epsilon\to 0$ defines a function $H(\beta)$ which diverges for $\beta<D_{H}$ and vanishes for $\beta>D_{H}$ where D_{H} is the Hausdorff dimension. The dynamic partition $\mathcal{A}^{(n)}$ is the covering belonging to $\mathcal{B}_\epsilon$ with $\epsilon=\lambda^n$ (where λ is the largest of the scales λ_i), for which the minimum is achieved. As a consequence the Hausdorff dimension satisfies $\lambda_1^{D_H}+\cdots+\lambda_s^{D_H}=1$ which implies $\mathcal{F}_{D}(0,-D_{H})=0$.

The uniform partitions $\mathcal{U}^{(n)}$ correspond to a tessellation of the unit cube into cubelets of side 2^{-n}. Replacing in the definition of the free energy the elements $A_{k_n,\ldots,k_1}$ of the dynamic partitions with the cubelets $c_i^{(n)}$ for $1\leqslant i\leqslant 2^{nd}$ and taking the base 2 logarithm we obtain the free energy $\mathcal{F}_{U}$ which reads

$$\mathcal{F}_U=\tau+\lim_{n\to\infty}\frac{1}{n}\log_2\sum_{i=1}^{2^{nd}}\mu^q(\mathcal{A}\cap c_i^{(n)}). \tag{2.6}$$

The exponents $\tau_{U}(q)$ for the uniform partitions are defined by $\mathcal{F}_{U}=0$ and read

$$\tau_U(q)=-\lim_{n\to\infty}\frac{1}{n}\log_2\sum_{i=1}^{2^{nd}}\mu^q(\mathcal{A}\cap c_i^{(n)}). \tag{2.7}$$

We shall consider the Legendre transform of $\tau(q)$ which enhances the deviations of $\tau(q)$ from a linear behaviour. Since $\tau(q)$ is concave $\mathrm{d}^2\tau/\mathrm{d}q^2<0$ its Legendre transform

$$f(\alpha)=\min_q(q\alpha-\tau(q))\qquad\longrightarrow\qquad\alpha=\frac{\mathrm{d}\tau}{\mathrm{d}q} \tag{2.8}$$

exists and is also concave. The following properties are an immediate consequence of the definition:

$$\max f(\alpha)=D_0\equiv D_{H}\qquad f(\alpha)=\alpha\quad\text{for }\alpha=D_1. \tag{2.9}$$

The interval $q<1$ is mapped into $[\alpha_1,\alpha_{-\infty}]$, the interval $q\geqslant 1$ into $[\alpha_{+\infty},\alpha_1]$ where $\alpha_1=D_1$ and $f'(\alpha_1)=1$. Since $q=\mathrm{d}f/\mathrm{d}\alpha$ the tangent is vertical at $\alpha_{\pm\infty}$ and the maximum of $f(\alpha)$ is at $\alpha_0>\alpha_1$ where $f(\alpha_0)=D_{H}$.

3. Multifractal measures

We have considered fractal measures on the unit square discretized by a $2^N\times 2^N$ matrix, where the integer entries g_i are the grey tones, ranging in the interval $[0,N_{gr}]$. The discretized measure on the unit square corresponds to the partition of order N.

The grey tone g_i is defined as the closest integer to $N_{gr}\,\mu(\mathcal{A}\cap c_i^{(N)})$. The exact measure of any cell $\mu(\mathcal{A}\cap c_i^{(N)})$ is replaced with g_i/G, where $G=\sum_{i=1}^{2^{2n}}g_i$ is very close to N_{gr}.

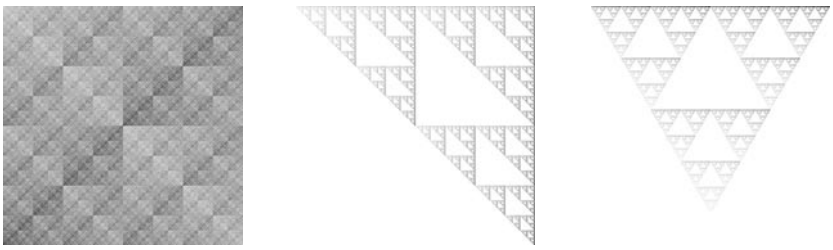

Figure 1. Measure I with support on the unit square, defined by the maps (3.2) with weights $p_1 = 0.225$, $p_2 = 0.275$, $p_3 = 0.265$, $p_4 = 0.235$ (left-hand side). Measure II with fractal support and dynamic partitions a subset of uniform partitions, defined by the maps (3.2) with weights $p_1 = 0.275$, $p_2 = 0.350$, $p_3 = 0.000$, $p_4 = 0.375$ (centre). Measure III with a generic fractal support defined by the maps (3.3) with weights $p_1 = 0.25$, $p_2 = 0.35$, $p_3 = 0.40$ (right-hand side).

For any lower-order partition $\mathcal{U}^{(n-1)}$ with $n \leqslant N$ we replace the measure $\mu(c_i^{(n-1)})$ with $g_i^{(n-1)}/G$ where $g_i^{(n-1)}$ is computed by summing the grey tones $g_{i'}$ of the four cells $c_{i'}^{(n)}$ whose union is $c_i^{(n-1)}$. By iterating the process, the grey tones for all the partitions from order n to order 0 is obtained. For the chosen value of n we consider the sequence

$$\tau_n(q) = -\frac{1}{n}\log_2 \sum_{i=1}^{2^{2n}} \left(\frac{g_i^{(n)}}{G}\right)^q \qquad 0 \leqslant n \leqslant N. \tag{3.1}$$

The exact spectrum $\tau(q)$ is given by the limit of $\tau_n(q)$ as $n \to \infty$. Three distinct classes were considered and shown in figure 1.

(I) Measures with support on the unit square. An example is the measure generated by the following maps suitably weighted

$$M_1 = \begin{pmatrix} \frac{1}{2}x \\ \frac{1}{2}y \end{pmatrix} \qquad M_2 = \begin{pmatrix} \frac{1}{2}x + \frac{1}{2} \\ \frac{1}{2}y \end{pmatrix} \qquad M_3 = \begin{pmatrix} \frac{1}{2}x \\ \frac{1}{2}y + \frac{1}{2} \end{pmatrix} \qquad M_4 = \begin{pmatrix} \frac{1}{2}x + \frac{1}{2} \\ \frac{1}{2}y + \frac{1}{2} \end{pmatrix}. \tag{3.2}$$

In this example the dynamic partitions are the uniform partitions, even though this is non-required.

(II) Measures with fractal support, whose dynamic partitions are a subset of uniform partitions. An example is obtained by setting to zero one of the weights of the maps (3.2).

(III) Measures with fractal support, with dynamic partitions which are not a subset of uniform partitions, such as those associated with the Sierpinski set

$$M_1 = \begin{pmatrix} \frac{1}{2}x \\ \frac{1}{2}y \end{pmatrix} \qquad M_2 = \begin{pmatrix} \frac{1}{2}x + \frac{1}{2} \\ \frac{1}{2}y \end{pmatrix} \qquad M_3 = \begin{pmatrix} \frac{1}{2}x + \frac{1}{4} \\ \frac{1}{2}y + \frac{\sqrt{3}}{4} \end{pmatrix}. \tag{3.3}$$

The $f(\alpha)$ spectra obtained from uniform and dynamic partitions are the same only if a measure has an Euclidean support (I), or a fractal support but its dynamic partitions are a subset of uniform partitions (II) [8]. Using suitable algorithms, based on integer arithmetics, the value of $\tau(q)$ is determined by a least square fit with respect to n of $n\tau_n(q)$ defined by (3.1).

The numerical analysis, carried out using a $2^9 \times 2^9$ grid on the unit square and $N_{gr} = 2^8$ grey tones, has shown that, for the measures of classes I and II the value of $\tau(q)$ given by the least square fit agrees with the exact value for any q (a typical accuracy is 10^{-3}), whereas for the generic fractal measures of class III the agreement for $q < 1$ is lost [8], see the right-hand

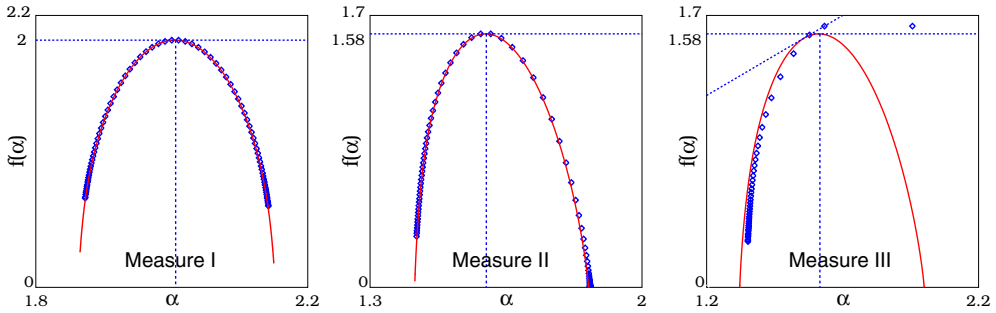

Figure 2. Local spectrum of exponents $f(\alpha)$ computed from uniform partitions (small circles) compared with the analytical result for the measures I, II, III shown in figure 1.

side of figure 2. The convention used for the reference frame in figure 1 is the standard one used in computer graphics:

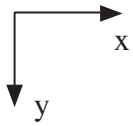

4. Measures with defects

We have considered another set of measures obtained by introducing defects in the generation process of the ordinary fractal measures. A way of generating the fractal measure consists in iterating the maps on an initial set $I \subset [0, 1]^2$, whose images $I_k = M_k(I)$ are disjoint.

At step n this cascade process generates the sets $I_{k_n,\ldots,k_1}$ whose weight is $p_{k_1} \ldots p_{k_n}$. In view of radiological applications we consider measures with defects, specified by a scale ϵ, a probability p and an attenuation factor η. The defect, which affects the dynamic partitions, whose diameter is less than ϵ, is introduced by choosing with probability p any element of the partition and by reducing the corresponding weight by a factor η. At any step the new pre-measure is defined after normalization. The way of generating a measure with defects is illustrated in figure 3 for a ternary Cantor set with weights $p_1 = 2/3$, $p_2 = 1/3$ where the defect parameters are $\epsilon = p = \eta = 1/2$. We compute the $\tau(q)$ spectrum on the limit measure (not on the sequence of pre-measures). The results concerning the properties of the measures are given in probability. As an example we consider the maps (3.2) with equal weights and $\eta = 0$ which produces a lacunar measure. The probability of getting an empty set is [3]

$$P_{\text{empty}} = t \quad t \text{ least positive solution of } t = ((1-p)(t-1)+1)^4. \tag{4.1}$$

When $p > 3/4$ we have $P_{\text{empty}} = 1$. For a smaller defect probability a non-empty set is generated with probability $1 - t$ and the expectation value of Hausdorff dimension of the support of the lacunar measure for $p < 3/4$ is

$$\mathsf{E}(D_H) = \frac{\log(4(1-p))}{\log 2}. \tag{4.2}$$

Cutoff. We have analysed several fractal measures with defects corresponding to the classes defined in section 3. It was found that $n\tau_n(q)$ follows a fairly linear law in n for $q > 0$, whereas for $q < 0$ a linear behaviour is found provided that one excludes all the scales above ϵ, which

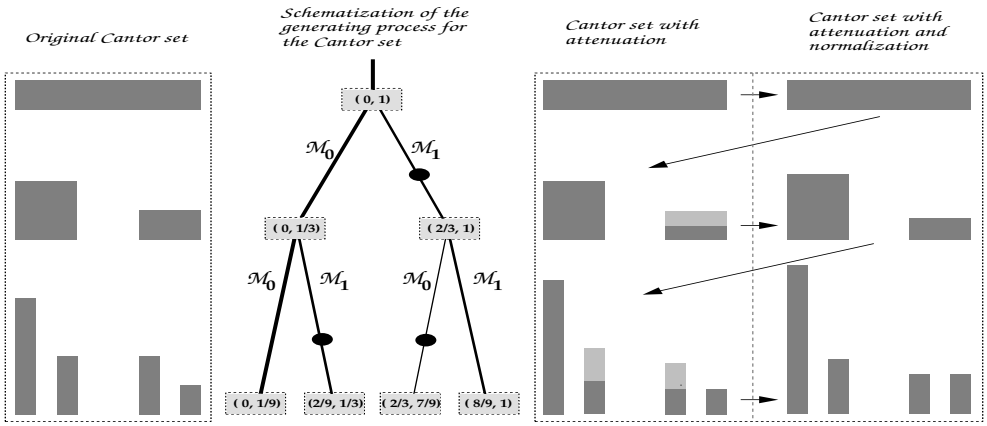

Figure 3. Generation of defects for the measure on a Cantor set.

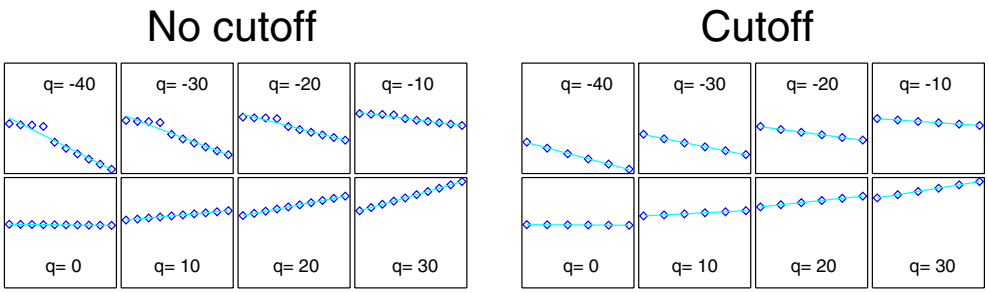

Figure 4. Graph of $\log_2 \sum (g_i^{(n)})^q = (N-n)\tau_n(q) + q \log_2 G - N\tau_N(q)$ versus $N-n$ and corresponding least square fitting line for the fractal measure defined by (3.2) with weights $p_1 = 0.225$, $p_2 = 0.265$, $p_3 = 0.235$, $p_4 = 0.275$ and defect appearing at the scale $\lambda = 2^{-6}$ with probability $p = 0.1$. All the figures of the left group refer to all the scales whereas the figures of the right group are obtained by discarding the scales smaller than ϵ.

is the scale at which the defect appears. In figure 4 the behaviour of $\log_2 \sum (g_i^{(n)})^q$ in the range $-40 \leqslant q \leqslant 30$ is shown: we compare, by drawing the least squares fitting line, the case where all the scales are retained and the case where a cutoff is introduced by discarding the scales smaller than ϵ (corresponding to $n \geqslant n_\epsilon$ if $\epsilon = 2^{-n_\epsilon}$). In figure 5 the effect of the cutoff on $f(\alpha)$ for a measure with defects is shown.

We recall that in the absence of defects the numerical $\tau(q)$ spectrum is accurate for any q, if the measure belongs to classes I or II. The presence of defects changes the local nature of the measure as shown by the spectrum of exponents. The application of the cutoff drastically changes the $\tau(q)$ spectrum for $q < 0$ and consequently the right part of the $f(\alpha)$ spectrum after its maximum. The spectrum $\tau(q)$ is a concave function for any choice of the cutoff and the Legendre transform is well defined. However, the application of a cutoff is necessary to have a good linear fit of $\log_2 \sum (g_i^{(n)})^q$ and a reliable determination of $\tau(q)$ for $q < 0$, see figure 4. The need to cutoff all the scales $n \geqslant n_\epsilon$ is not surprising since at $n = n_\epsilon$ there is a sudden change. For $n < n_\epsilon$ the weights of the sets $I_{k_n,\ldots,k_1}$ are less sensitive to the fluctuations affecting a single realization of the measure with defects. The dimensions spectrum is evaluated for any realization of the measure with defects. We expect that the Legendre transform $f(\alpha)$ of the $\tau(q)$ spectrum computed with the cutoff is capable of detecting the presence of defects.

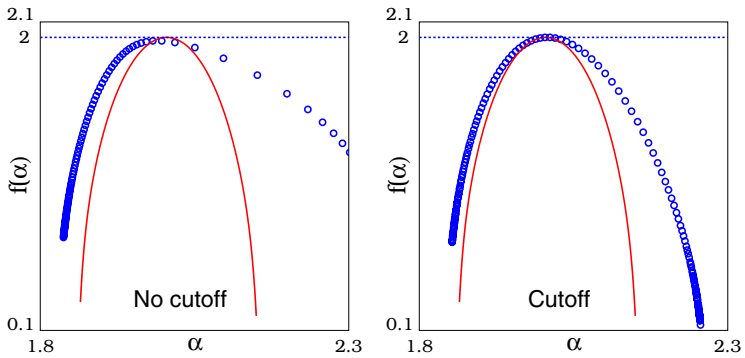

Figure 5. Spectrum of exponents for the measure (3.2) with defects inserted at scale $\epsilon = 2^{-6}$ with probability $p = 0.1$ (small circles) and the same spectrum for the measure with no defects (curve). The left-hand figure is obtained by keeping all the scales, whereas in the right-hand one the scales smaller than ϵ are discarded.

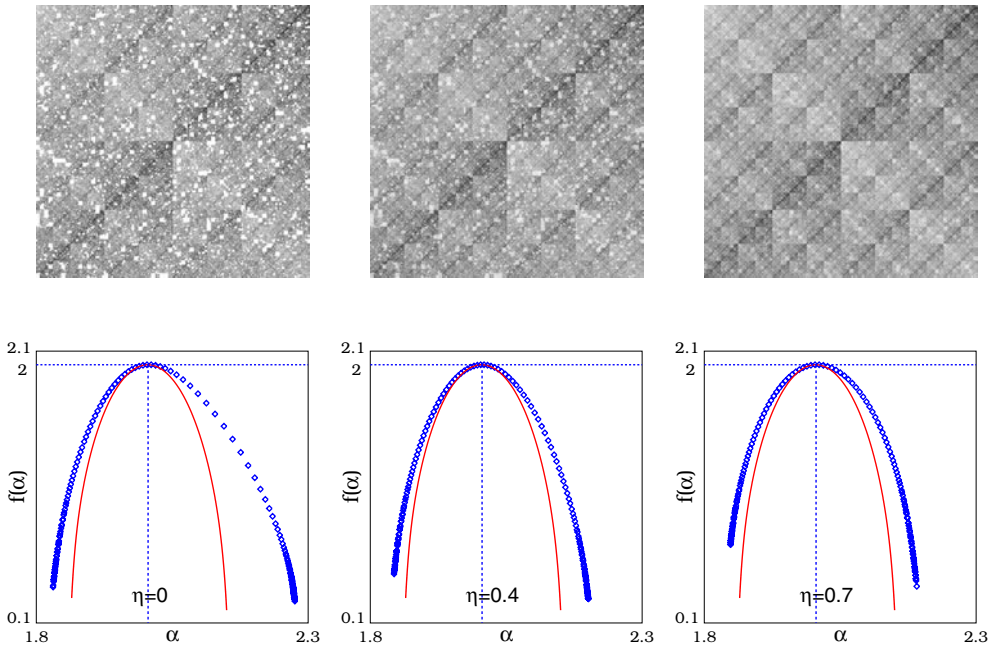

Figure 6. Fractal measure with defects corresponding to the maps 3.2 with weights $p_1 = 0.225$, $p_2 = 0.275$, $p_3 = 0.265$, $p_4 = 0.235$. The defect scale and probability are $\epsilon = 2^{-6}$, $p = 0.05$. From left to right the measure and the corresponding $f(\alpha)$ are shown for attenuation factors $\eta = 0$, 0.4, 0.7. For comparison the $f(\alpha)$ of the standard measure ($p = 0$) is shown (continuous curve).

The choice of an attenuation factor η in the range [0, 1] generates a family of probabilistic fractal measures whose spectrum $f(\alpha)$ varies continuously from the lacunar $\eta = 0$ to the standard measure $\eta = 1$. As shown by figure 6, when η increases from left to right, the width of the spectrum decreases until the standard spectrum is recovered. This result is consistent with a spread of the local exponents, caused by the introduction of defects. The low defect probability $p = 0.05$, chosen in figure 6 gives an almost zero probability of getting an empty set

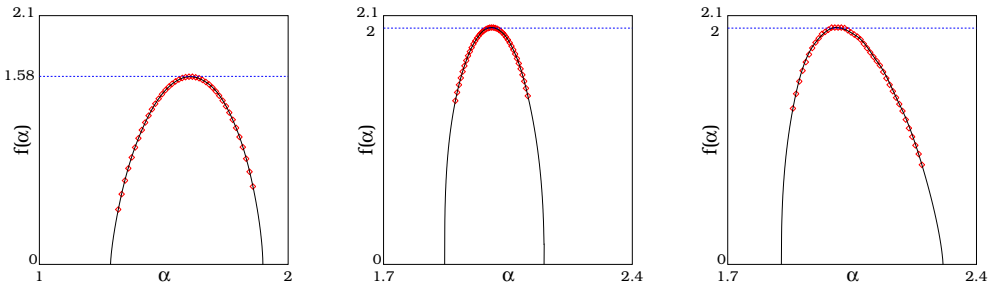

Figure 7. Extrapolation by cubic splines of the $f(\alpha)$ spectrum. Measure with fractal support generated by the map (3.2) with weights $p_1 = 0.32$, $p_2 = 0.27$, $p_3 = 0.0$, $p_4 = 0.41$ (left side). Measure with support $[0, 1] \times [0, 1]$ generated by the map (3.2) with weights $p_1 = 0.225$, $p_2 = 0.275$, $p_3 = 0.265$, $p_4 = 0.235$ (centre); the same measure with lacunes appearing at scales smaller than $\epsilon = 2^{-6}$ and probability $p = 0.1$ (right-hand side).

($P_{\text{empty}} = 6.3 \times 10^{-6}$) when $\eta = 0$, whereas the expectation value of the Hausdorff dimension of the set is $\mathsf{E}(D_H) = 1.926$. When $\eta \to 0$ the reliability of the uniform partition algorithms to compute $\tau(q)$ becomes doubtful for $q < 0$, because we are approaching a limit in which the support of the measure is a fractal set. We believe that, for very low defect probabilities $p \ll 1$, uniform partitions are still reliable for small η, but a check with the algorithms [9, 10], convergent for $q < 0$, should be made.

If the measure is deterministic no negative values of $f(\alpha)$ are allowed. Random measures may lead to negative values of $f(\alpha)$. In this case $f(\alpha)$ can vanish, and the values of α where it occurs correspond to values of q such that $\tau(q)$ has a tangent straight line passing through the origin. For the measures with defects we considered having $\eta > 0$ the occurrence for some realization of negative values of $f(\alpha)$ is a very rare event.

Moments. In order to evaluate in a quantitative way the effect of the size and probability of the defects it is convenient to introduce a set of moments, which characterize the shape of the spectrum $f(\alpha)$. To this end we need to interpolate the spectrum and extrapolate it to cover the whole interval $\alpha_{\pm\infty}$, where $f(\alpha)$ is defined. This can be achieved by using cubic splines. If the generalized dimensions are computed in the interval $[q_-, q_+]$, which is mapped into $[\alpha_+, \alpha_-] \subset [\alpha_{+\infty}, \alpha_{-\infty}]$, the cubic splines are evaluated with the additional constraint $f'(\alpha_\pm) = q_\pm$. The unknown endpoints $\alpha_{\pm\infty}$ are determined by imposing that the interpolating function $f(\alpha)$ vanishes with a vertical tangent $f'(\alpha_{\mp\infty}) = \pm\infty$. In the intervals $[\alpha_{+\infty}, \alpha_+]$ and $[\alpha_-, \alpha_{-\infty}]$ the interpolating function has been chosen of algebraic type $C_+(\alpha - \alpha_{+\infty})^{\beta_+}$, $C_-(\alpha_{-\infty} - \alpha)^{\beta_-}$ respectively, where the coefficients $C_\pm$, the exponents $\beta_\pm$ and the unknown ends $\alpha_{\pm\infty}$ are determined by imposing the continuity at $\alpha_\pm$ of the function and its first two derivatives (C^2 interpolation).

An equivalent procedure consists in imposing at every interpolation point the continuity of the function and its first derivative $f'(\alpha) = q$, which is explicitly known (C^1 interpolation). Comparable results are obtained from both methods; the results presented here refer to the second procedure.

For an IFS measure, the extrapolation, shown by figure 7, agrees with the exact result within the graphical resolution. A corresponding lacunar measure exhibits a significant widening of the $f(\alpha)$ spectrum. The lacunarity changes the moments by about one order of magnitude, see figure 8. For the $f(\alpha)$ values plotted in the central frame of figure 7 the moments with $n \leqslant 4$ are $\mu_2 = 5 \times 10^{-3}$, $\mu_3 = 1.1 \times 10^{-5}$, $\mu_4 = 5.1 \times 10^{-5}$. For the $f(\alpha)$ of the corresponding

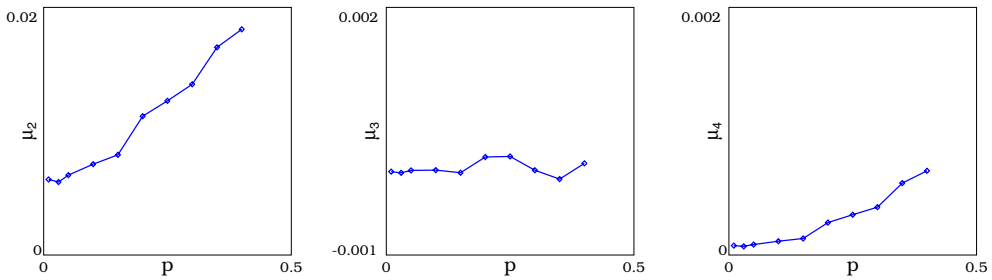

Figure 8. Second, third and fourth moments of the $f(\alpha)$ spectrum as a function of the defects probability p. The probability of having an empty set increases with p and is below 0.03 for the quoted values ($P_{\text{empty}}(0.2) = 0.0016$, $P_{\text{empty}}(0.4) = 0.031$).

lacunar measure plotted in the right frame of figure 7: $\mu_2 = 1.2 \times 10^{-2}$, $\mu_3 = 2.5 \times 10^{-4}$, $\mu_4 = 3.1 \times 10^{-4}$.

5. Biomedical applications

In this section we consider an application of multifractal analysis to the cancellous bone radiographs, showing that the $f(\alpha)$ spectrum of local exponents can discriminate between the normal and osteoporotic tissue, where lacunar type defects are present.

5.1. Bone structure

Bone structure consists of a cortical layer of compact bone that surrounds an inner core of cancellous bone, composed of a network of trabeculae, mainly oriented along stress lines. In the osteoporotic bone, resorption prevails over neodeposition, so that both cortical and cancellous bone decrease in overall mass. However, the tendency of osteoporotic bone to fracture is due mainly to an altered distribution of bony trabeculae in space. The thinning of trabeculae *per se* is not sufficient to determine bone fragility, whilst alterations of the three-dimensional texture of the trabecular bone appears to be related to the tendency of osteoporotic bone to fracture. In conclusion the strength and solidity of cancellous bone does not exclusively depend on bone mineral density (BMD) but also on trabecular architecture. BMD can be evaluated in a quantitative way by a non-invasive technique, while this is not the case for trabecular architecture.

5.2. Multifractal analysis of normal cancellous bone

A high-resolution post-mortem radiography of a normal vertebra of a young subject is shown in figure 9. Analogous resolution cannot be achieved in routine diagnostic radiology. Such image has been used as a standard of cancellous bone architecture, in order to show the properties of the measure specified by the spectrum $f(\alpha)$ of local exponents shown in figure 10.

The spectrum, computed with different cutoffs on the lower scales, appears to be stable and smooth so that a spline extrapolation to the missing part can be performed in order to evaluate the moments, see figure 11.

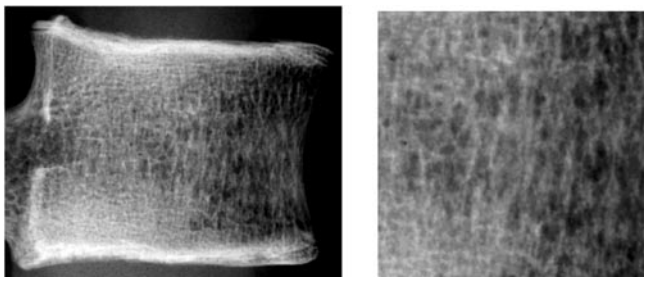

Figure 9. Image of trabecular bone (vertebra) (left-hand side). Magnified element of the same image.

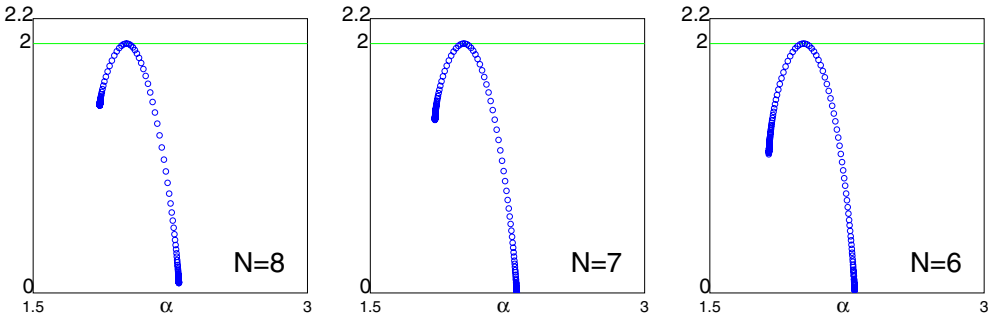

Figure 10. Function $f(\alpha)$ for the image shown in the right-hand side of figure 9. The variable q was chosen in the interval $[-30, 30]$ and the scales used for the extrapolation of $\tau(q)$ were chosen to be in the range $[2^{-N}, 2^0]$ where $N = 8$ (left-hand side), $N = 7$ (centre), $N = 6$ (right-hand side).

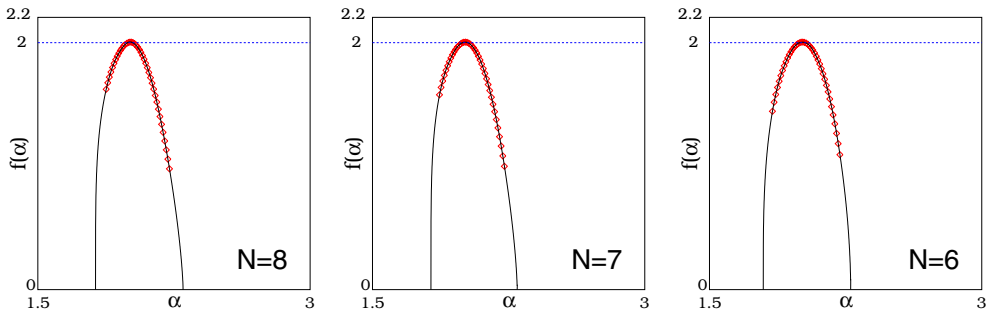

Figure 11. Splines extrapolation for the spectra shown in figure 10.

5.3. Multifractal analysis of osteoporotic cancellous bone

Osteoporosis has been considered to depend on a decrease in bone mass which affects its strength and increases the risk of fracture. Therefore methods determining BMD have been utilized to identify the patients at risk of fracture. However, it has been demonstrated that BMD measurements alone may be insufficient to determine the actual solidity of the cancellous bone, which mainly depends on trabecular architecture.

Changes in trabecular architecture of cancellous bone strictly related to osteoporotic processes can be clearly determined by invasive methods such as histomorphometry of bone

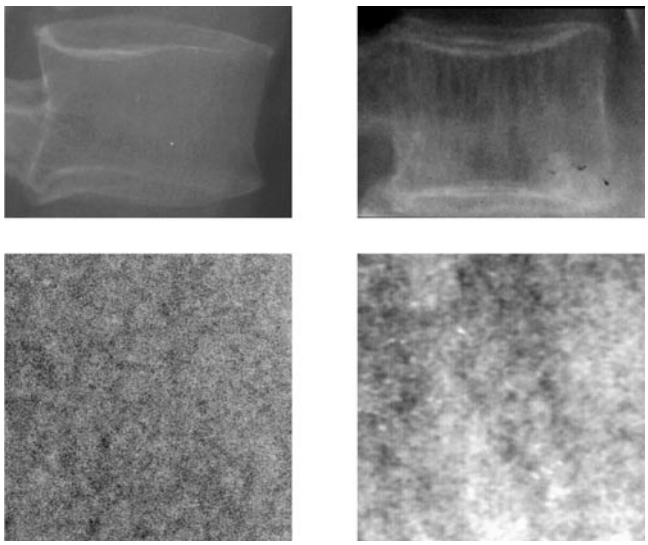

Figure 12. Image of normal bone (upper left) and of osteoporotic bone (upper right). Element of normal bone (lower left) and of osteoporotic bone (lower right).

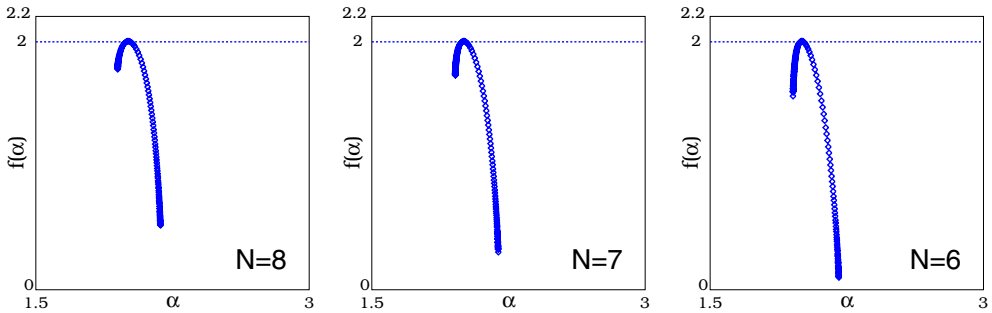

Figure 13. Function $f(\alpha)$ for the image shown in the left-hand side of figure 12, corresponding to a normal bone. The variable q was chosen in the interval $[-30, 30]$ and the scales used for the extrapolation of $\tau(q)$ were chosen to be in the range $[2^{-N}, 2^{0}]$ where $N = 8$ (left-hand side), $N = 7$ (centre), $N = 6$ (right-hand side).

biopsies. In order to measure the same parameters in clinical radiographs, which represent a bi-dimensional projection of a complex 3D structure, fractal geometry could represent a suitable approach. Some studies have appeared describing the application of fractal dimension analyses to radiographs of human bone [14–18]. In figure 12 we show two radiographs of a vertebra, the left-hand side corresponding to a normal case like the one shown in figure 9, the right-hand side to an osteoporotic bone. In figure 13 we show the $f(\alpha)$ spectrum of the normal bone and in figure 14 the corresponding spectrum of the osteoporotic bone. Having examined several other images we can conclude that spectra for the normal and osteoporotic bone exhibit a different shape: the curve $f(\alpha)$ is definitely wider in the second case, in agreement with an increase of the lacunarity of the body.

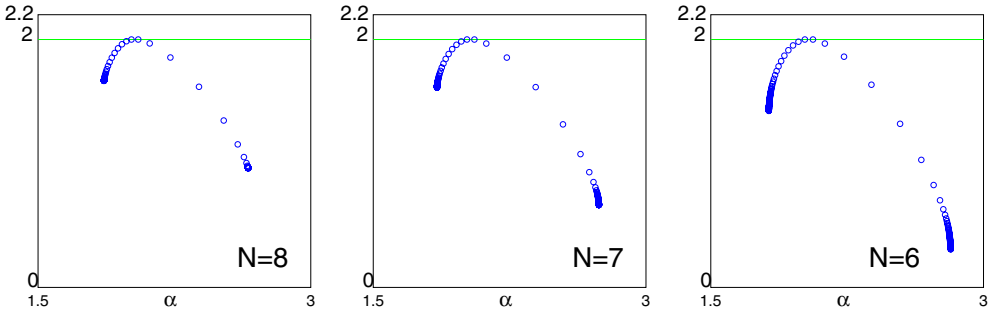

Figure 14. Function $f(\alpha)$ for the image shown in right-hand side of figure 12, corresponding to an osteoporotic bone. The variable q was chosen in the interval $[-30, 30]$ and the scales used for the extrapolation of $\tau(q)$ were chosen to be in the range $[2^{-N}, 2^{0}]$ where $N = 8$ (left-hand side), $N = 7$ (centre), $N = 6$ (right-hand side).

6. Conclusions

We have examined a family of IFS measures with defects, showing that the $f(\alpha)$ spectrum of local exponents widens monotonically with the attenuation factor of the measure η, reaching a maximum when the defect is a lacuna ($\eta = 0$). The moments of the measure allow one to determine quantitatively this dependence on η. An image may be considered as a fractal measure specified by a given uniform partition. In this case the $f(\alpha)$ spectrum extracts more information with respect to the grey tones distribution and to the box counting dimension. We have used the $f(\alpha)$ spectrum of local exponents, to compare normal and osteoporotic bone radiographs. In high-resolution radiographs the cancellous bone structure emerges very neatly. The osteoporotic bone radiographs exhibit a widening of the $f(\alpha)$ spectrum similar to the IFS measures with defects, since the decrease of the bone mass determines a rarefaction of the cancellous bone. The algorithms based on uniform partitions are fast and allow real time analysis of high-resolution radiographs. As a consequence the spectrum of local exponents could be used to discriminate by radiographs the normal and osteoporotic cancellous bone, in order to identify the patients at risk of fracture.

Acknowledgment

The authors wish to thank one of the referees for very constructive criticism, which allowed us to improve quite significantly the text of this paper.

References

[1] Grassberger P and Procaccia I 1983 Characterization of strange attractors *Phys. Rev. Lett.* **50** 346
[2] Grassberger P and Procaccia I 1983 Scaling structure and thermodynamics of strange sets *Physica* D **9** 189
[3] Falconer K J 1990 *Fractal Geometry* (New York: Wiley) pp 230–3
[4] Jensen M H, Kadanoff L P and Procaccia L 1987 Measuring the strangeness of strange attractors *Phys. Rev.* A **36** 1409
[5] C Beck and F Schlögel 1993 *Thermodynamics of Chaotic Systems* (Cambridge: Cambridge University Press)
[6] Collet P, Lebowitz K J L and Porzio A 1987 The dimension spectrum of some dynamical systems *J. Stat. Phys.* **47** 609
[7] Pesin Y and Weiss H 1996 On the dimension of deterministic and random Cantor-like sets *Commun. Math. Phys.* **182** 105

[8] Campagna S and Turchetti G 1999 Dimensions spectra of fractals measures from uniform partitions and correlation integrals *J. Phys. A: Math. Gen.* **32** 7989
[9] Pastor-Satorras R and Riedi R H 1996 Numerical estimates of the generalized dimensions of the Hénon attractor for negative *q J. Phys. A: Math. Gen.* **29** L391
[10] Struzik Z R 1998 Removing divergences of negative moments of the multi-fractal partition function with the wavelet transformation *Technical Report* CWI Netherlands INS-R9803
[11] Barnsley M 1988 *Fractals Everywhere* (New York: Academic)
[12] Falconer K J 1986 Random fractals *Math. Proc. Camb. Phil. Soc.* **100** 559
[13] Lespessailles E C, Roux J P, Benhamou C L, Arlot M E, Eynard E, Harba R, Padanou C and Meunier P J 1998 Fractal analysis of bone texture on os calcis radiographs compared with trabecular microarchitecture analyzed by histomorphometry *Calcif. Tissue Int.* **63** 121
[14] Caligiuri P, Giger M L and Favus M 1994 Multifractal radiographic analysis of osteoporosis *Med. Phys.* **21** 503
[15] Fazzalari N L and Parkinson I H 1998 Fractal properties of cancellous bone of the iliac crest in vertebral crush fracture *Bone* **23** 53
[16] Weinstein R and Majumdar S 1994 Fractal geometry and vertebral compression fractures *J. Bone Miner. Res.* **9** 1797
[17] Chung H W, Chu C C, Unterriser M and Werli F W 1994 On the fractal nature of trabecular structure *Med. Phys.* **21** 1535
[18] Link T M, Majumdar S, Augat P, Lin J C, Newitt D, Lu Y, Lane N E and Genant H K 1998 In vivo high resolution MRI of the calcaneous: differences in trabecular structure in osteoporosis patients *J. Bone Miner. Res.* **13** 1175